Journal of Materials Chemistry A

ROYAL SOCIETY OF CHEMISTRY

PAPER

View Article Online
View Journal | View Issue

Cite this: J. Mater. Chem. A, 2025, 13, 27524

Base-mediated exfoliation of quinoline-linked covalent organic frameworks for heavy metal ion adsorption†

Yongjie Xu,[ab] Yang Liu,[c] Xue Wang,[a] Haofan Yang,[a] Peiying Wang,[a] Weiwei Zhang,[d] John W. Ward *[a] and Andrew I. Cooper *[a]

Received 14th May 2025
Accepted 21st July 2025

DOI: 10.1039/d5ta03899e

rsc.li/materials-a

Multicomponent reactions that combine sequential reversible and irreversible bond forming reactions are efficient methods for the synthesis of robust covalent organic frameworks (COFs) with high crystallinity and stability. Here, we report a mild synthetic method for the synthesis of quinoline-linked covalent organic frameworks (Qu-COFs) using a multicomponent Doebner reaction. These Qu-COFs have high stability, crystallinity, porosity, and good wettability. The unique quinoline-4-carboxylic acid linkage resulting from the Doebner reaction enables ion insertion and exfoliation of bulk Qu-COF under mild conditions to give 2D nanosheets (Qu-CONs). Furthermore, the exfoliated Qu-CONs exhibit ultrafast cadmium ion uptake. Our work provides a mild and efficient method for synthesizing stable, functionally diverse 2D nanosheets and further expands the potential applications of COFs.

Introduction

Covalent organic frameworks (COFs) are crystalline, porous, two-dimensional or three-dimensional polymers with tunable topology and functionality.[1] COFs have attracted interest in areas such as adsorption, gas storage[2] and gas separation,[3] catalysis,[4,5] and energy conversion[6] and storage.[7,8] Reversible covalent linkages that allow for error-correction processes and interlayer π–π interactions between 2D layers are key for the successful construction of crystalline 2D COFs.[9] However, the low chemical stability resulting from reversibility and the poor processibility of the resulting bulk powders can limit the practical applications of 2D COFs.[10,11] By increasing dispersibility, it is possible to form COF nanosheets.[12–14] Several methods have been investigated for the preparation of nanosheets by exfoliation of bulk 2D COFs.[15,16] Exfoliated nanosheets have benefits that include exposed surface functionalities and more accessible active sites. COF nanosheets have therefore been used for applications such as separation and energy storage applications.[17–20] Because of the weak chemical stability and strong interlayer interactions of most reported COFs, it is still challenging to find a general strategy to achieve exfoliation.[21,22] Several research groups have reported in-depth studies of how the stacking structure and interlayer interaction influence exfoliation of 2D COFs, but no general rules apply.[23–25] Hence, development of robust 2D COF nanosheets will have significant implications for the practical applications of COFs.

Multicomponent reactions (MCRs) are efficient and atom economical reactions involving three or more reactants to give a single product in a one-pot process. MCRs are ideal candidates for the synthesis of stable, crystalline COFs because they can combine reversible covalent bond-forming reactions to confer crystallinity with irreversible steps that confers stability.[26] Furthermore, due to the introduction of a third component, MCRs can be an efficient method for the structural diversification and functionalization of COFs. The first reported COF synthesis using a multicomponent reaction was by Wang and co-workers using the Debus reaction.[27] Subsequently, several groups, including our own,[28] have reported COF syntheses using multicomponent reactions, but challenges still remain. Quinoline and tetrahydroquinoline-linked COFs have been synthesised using both multicomponent and post-synthetic Povarov reactions, which require strong Lewis acids or high temperatures.[29–31] The Doebner reaction is an alternative multicomponent reaction for the synthesis of quinolines which uses a combination of amine, aldehyde and an α-ketoacid or α-ketoester functionality under mild reaction

[a]Leverhulme Research Centre for Functional Materials Design, Department of Chemistry and Materials Innovation Factory, University of Liverpool, Liverpool L69 7ZD, UK. E-mail: aicooper@liverpool.ac.uk; john.ward@liverpool.ac.uk

[b]Ningbo Institute of Digital Twin, Eastern Institute of Technology, Ningbo, Zhejiang 315200, P.R. China

[c]State Key Laboratory of Polymer Materials Engineering, College of Polymer Science and Engineering, Sichuan University, Chengdu 610065, P.R. China

[d]Key Laboratory for Advanced Materials and Institute of Fine Chemicals, Joint International Research Laboratory of Precision Chemistry and Molecular Engineering, Feringa Nobel Prize Scientist Joint Research Center, Frontiers Science Center for Materiobiology and Dynamic Chemistry, School of Chemistry and Molecular Engineering, East China University of Science and Technology, Shanghai 200237, P.R. China

† Electronic supplementary information (ESI) available. See DOI: https://doi.org/10.1039/d5ta03899e

conditions.[32] Moreover, the third component can be well designed for the additive functionalities of the products, therefore, Doebner reaction is an efficient tool for both novel COFs synthesis and functionalisation for specific applications.[34,35]

Here, we report the synthesis of stable quinoline-linked COFs using a three-component Doebner reaction. The synthetic flexibility of the Doebner reaction enabled access to quinoline-linked COFs (Qu-COFs) from both one-pot synthetic and post-synthetic methods. The quinoline-4-carboxylic acid linking groups in the framework, which are unique to the Doebner reaction, allows efficient exfoliation of the bulk material to 2D nanosheets under mild conditions. Exfoliated Qu-CONs were further used as sorbents for cadmium removal and showed performance that was superior to bulk imine COFs.

Results and discussion

The Doebner reaction is an efficient, operationally simple multicomponent reaction for the synthesis of quinoline-4-carboxylic acids. The proposed mechanism begins with the condensation of an amine and an aldehyde to form an imine-based compound (**1**) followed by nucleophilic attack of pyruvic acid and Pictet–Spengler-like cyclisation to afford hydroquinone (**3**) after aromatization and dehydration steps. Oxidation then forms the desired quinoline-4-carboxylic acid (**4**) irreversibly (Fig. 1a). The multicomponent Doebner reaction was used to construct quinoline-linked covalent organic frameworks (Qu-COFs) by both one-pot and two-step post-synthetic methods, respectively. For the one-pot method, we selected 4,4′,4″-(1,3,5-triazine-2,4,6-triyl)tribenzaldehyde (TAPT) and 2,5-dimethoxy terephthalaldehyde (DMTPA), and 1,3,5-tri(4-aminophenyl)benzene (TAPB) monomers to react with pyruvic acid in the presence of 6 M AcOH and chloranil as oxidant to give Qu-COFs 1a and 2a. After investigating these initial reaction conditions, we found Qu-COF-2a was less crystalline so decided to optimize on this COF. After screening solvents, cosolvents, oxidants, concentration, stoichiometry, and temperature (see ESI†), the optimal reaction conditions afforded Qu-COF-2a in 85% yield (Scheme S3 and Table S1†). This yield is comparable with the model compound M_1 prepared under the same reaction conditions (Scheme S1†). We found that the choice of oxidant affected the crystallinity, with chloranil giving the highest crystallinity (Fig. S3 and S4†). The

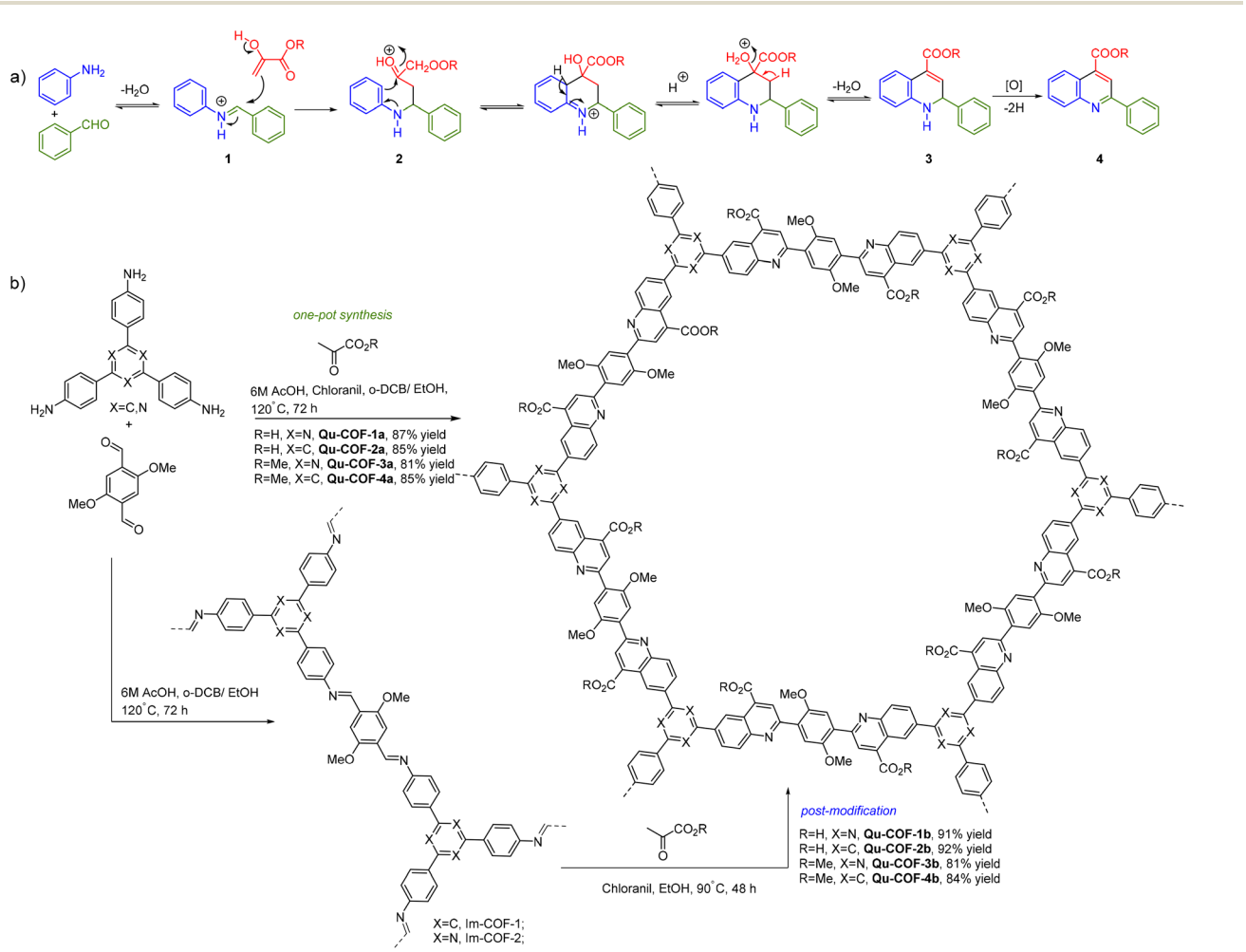

Fig. 1 Synthesis of quinoline-linked covalent organic frameworks (Qu-COFs) by a multicomponent Doebner reaction. (a) Proposed mechanism of quinoline formation; (b) synthesis of Qu-COFs *via* one-pot synthesis route and two-step post-modification route.

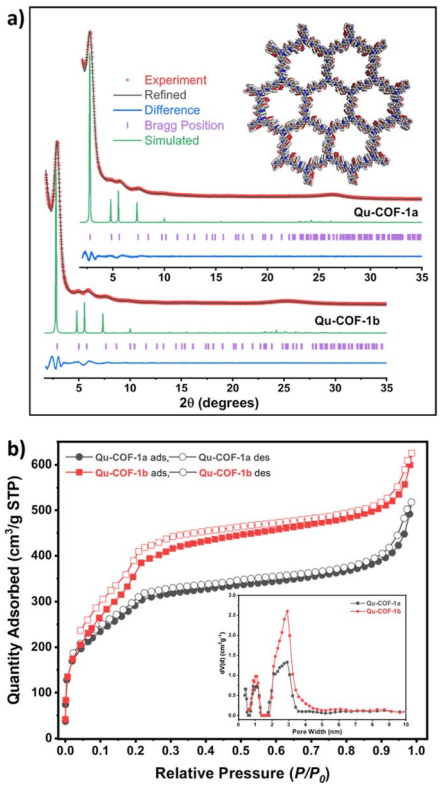

Fig. 2 (a) Structural models for Qu-COF-1a&b with eclipsed AA stacking patterns, shown parallel to the pore channel along the crystallographic *c* axis (inset). Experimental diffraction patterns (red), profiles calculated from Pawley fitting (black) showing the residual (blue), and pattern simulated from the structural model (green). Reflection positions are shown by tick marks (purple). (b) Nitrogen adsorption and desorption isotherms for Qu-COF-1a (black) and Qu-COF-1b (red) recorded at 77 K (filled symbols = adsorption; open symbols = desorption). Insert is the pore size distribution calculated by NL-DFT method.

two-step post-synthetic method was initially investigated with Im-COF-1 (Fig. 1). After screening reaction conditions, we found that 3 equivalents of pyruvic acid in the presence of 6 M AcOH and chloranil in neat ethanol at 90 °C afforded Qu-COF-1b in 91% yield (Scheme S3†). The crystallinity and surface areas obtained from both methods are comparable (Fig. 2). To investigate the scope of the pyruvate component in both methods we also used methyl pyruvate to produce Qu-COF-Qu-COF-3a & b and Qu-COF-4a & b respectively (Schemes S3 and S5–8†). Qu-COFs 1–4 were all synthesized under mild conditions in high yields and exhibited good crystallinity.

Powder X-ray diffraction (PXRD) was used to characterize the frameworks, based on comparison with optimized, idealized structural models of the expected networks (Fig. 2a and 3). The diffraction patterns of all frameworks exhibited characteristic reflections that indicated ordered layers within the structure. In all Qu-COFs cases, the diffraction patterns were more consistent with the eclipsed AA stacking arrangement, rather than a staggered AB stacking, although the number of peaks observed was modest. An intense low angle peak is present in all Qu-COFs which correspond to the (100) reflection plane (Fig. 2a and 3a–f). The diffraction peaks were relatively broad, as is common for COFs of this type that feature stable, irreversible bonds. The diffraction patterns of Qu-COF-1a & b and Qu-COF-3a & b show a series of peaks at 2.89°, 4.93°, 5.94° and 7.66°, corresponding to (100), (110), (200) and (210) reflection planes, respectively (Fig. 3a). Similarly, the PXRD patterns of Qu-COF-2a & b and Qu-COF-4a & b exhibit four peaks at 2.78°, 4.84°, 5.60° and 7.42°, belonging to the (100), (110), (200) and (210) facets, respectively. Compared with calculated structural models of eclipsed AA-stacking, all the experimental PXRD curves of Qu-COFs are in broad agreement with simulation patterns. The unit cell parameters were determined by Pawley refinements with respect to the experimental diffraction patterns. The differences between the experimental and the simulated PXRD patterns were small, and the refined curves show close matching for all reflection positions with reasonable converged *R* factors (R_{wp} and R_p), again indicating agreement of experimental data and simulation models. During the modelling of the Qu-COFs, we compared the *c* values with their parent Im-COFs and found that Qu-COFs have a larger interlayer stacking distance (3.8–4.2 Å) and are slightly twisted out of the plane causing much larger *d*-spacing (Fig. S6† and 3a–f).

The formation of the quinoline linkages was confirmed by Fourier-transformed infrared (FT-IR) spectroscopy (Fig. S7†). One salient feature of the quinoline-4-carboxylic acid or ester is the carbonyl (C=O) stretch at 1700 cm^{-1} which appears in all Qu-COFs. The appearance of a C=O stretch coincides with the disappearance of C=N stretch from the imine bond at 1614 cm^{-1}. The same was observed for the model compound M_1. X-Ray photoelectron spectrometry (XPS) measurements confirmed the elemental configurations of Qu-COFs, showing the presence of C 1s, N 1s, and O 1s (Fig. S8†). Compared with the N 1s peak (399.0 eV) from the imine bond of Im-COFs, the N 1s peak of Qu-COFs is red-shift to 400.0 eV, which corresponds to quinoline-*N* (Fig. S9 and S11b†), indicating the formation of quinoline rings. Solid-state ^{13}C cross polarization magic angle spinning (CP/MAS) NMR spectroscopy shows a shift of the sp^3-hybridised carbon from the methoxy group of Qu-COFs from 52 ppm to 56 ppm of the corresponding Im-COFs (Fig. S10†). Such shift might come from the high electron density on the quinoline rings. Compared with Im-COFs, the shift peak at 151 ppm of Qu-COFs can be assigned to the 2-quinolyl carbon and the peak at around 167 ppm can be assigned to the carbon from the carboxylic acid. This signal can be enhanced dramatically by using ^{13}C-labelling Qu-COF-2a using ^{13}C-labelled pyruvic acid (Scheme S9 and Fig. S11†). These observations are consistent in all of Qu-COFs synthesized (Fig. S12–S16†), and provide evidence of successful quinoline linkage formation.

The surface area and porosity of Qu-COFs were measured by nitrogen adsorption–desorption analysis at 77 K (Fig. S17†). The Brunauer–Emmett–Teller (BET) surface areas of Qu-COFs made by the one-pot method (Qu-COF-1–4a) were 1047, 436, 888 and 415 $m^2\ g^{-1}$, respectively. The BET surface areas of Qu-COFs synthesised by post-modification methods (Qu-COF-1–4b) were 1316, 912, 998 and 643 $m^2\ g^{-1}$, respectively. The pore size distributions were calculated using nonlocal density functional theory (NL-DFT), showing pore size distributions for Qu-COFs

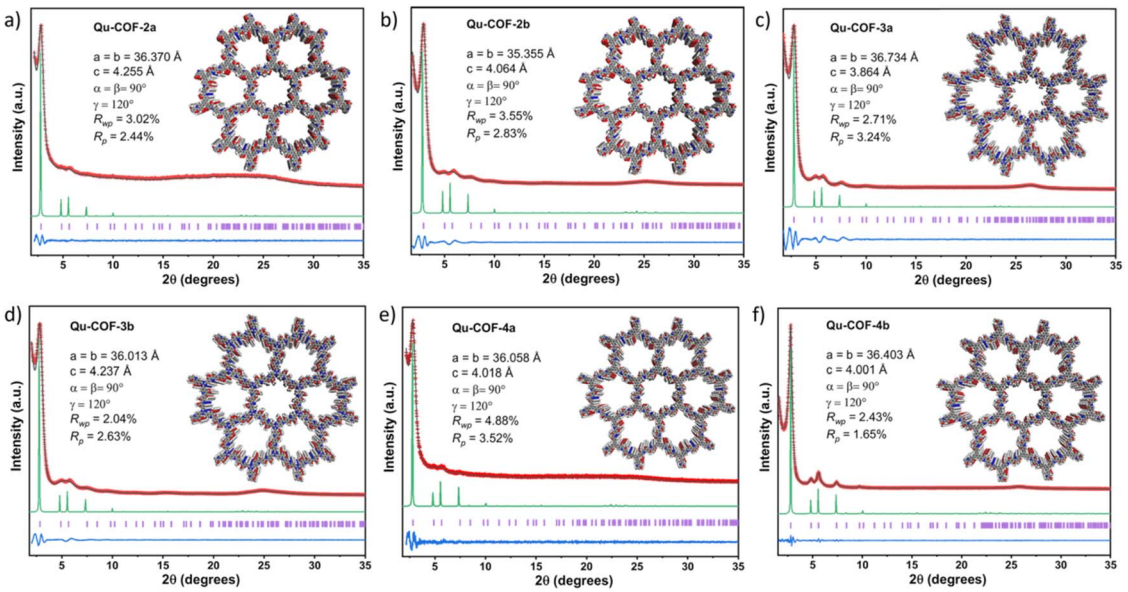

Fig. 3 Crystal structures of Qu-COF-2a & b–4a & b (a–f). Structural models for all the Qu-COFs with eclipsed AA stacking patterns, shown parallel to the pore channel along the crystallographic *c* axis (inset). Experimental diffraction patterns (red), profiles calculated from Pawley fitting (black) showing the residual (blue), and pattern simulated from the structural model (green). Reflection positions are shown by tick marks (purple).

centered at around 2.6 nm, which is consistent with the PXRD results. The pore size distributions of Qu-COFs are close to their corresponding Im-COFs, indicating the same topology for all Qu-COFs. From the images of field-emission scanning electron microscopy (FE-SEM) and high-resolution transmission electron microscopy (HR-TEM), both Qu-COF-1 & 3 and Im-COF-1 show a rod-like structures while Qu-COF-2 & 4 and Im-COF-2 show a microsphere-like structure (Fig. S18–S26†). Energy dispersive X-ray spectrum (EDS) elemental mapping of Qu-COFs show a homogenous elemental distribution of carbon, nitrogen and oxygen within the skeleton structures, indicating the successful introduction of quinoline functionality from the Doebner reaction (Fig. S27 and S28†).

Solid-state UV/visible adsorption spectra was used to assess the optical properties of Qu-COFs (Fig. S29†). The spectra show that all the COFs can absorb light in the UV and visible regions. The optical band gaps of Qu-COFs 1a & b–2a & b were calculated to be 1.58, 1.62, 1.75 and 1.69 eV, respectively. These are narrower than their respective Im-COF-1 and Im-COF-2 (2.35 and 2.31 eV) (Fig. S30†). Also, in comparison with Im-COFs, these Qu-COFs exhibit a red shift of their absorption edge to longer wavelength and enhanced intensity of visible-light absorption.

Thermogravimetric analysis (TGA) revealed Qu-COFs are thermally stable up to approximately 300 °C. We propose the weight loss at 300 °C is due to decarboxylation of the carboxylic acids (Fig. S31 and S32†). The stability of Qu-COFs was examined in common solvents, such as water, acetone, tetrahydrofuran (THF), *N*,*N*-dimethylformamide (DMF), chloroform, aqueous KOH (6 M), and HCl (6 M). Loss of crystallinity was observed in each case, but the FT-IR spectra remain unchanged indicating retention of the atomic-level connectivity (Fig. S33 and S34†). Considering the quinoline linkage should be stable under these conditions, we hypothesized that this loss of crystallinity might be due to the unique structural features of the quinoline-4-carboxylic acid group resulting from the Doebner reaction disrupting the interlayer interaction.

Immersion of Qu-COF-2a in 6 M KOH solution for 24 hours resulted in a boarder (001) peak from 15° to 25° with maximum at around 20° in the PXRD. This indicated a larger *d*-spacing of interlayers and exfoliation of layers in the basic solution[33] (Fig. S5†). We propose that the carboxylic acid groups contained in the quinoline-4-carboxylic acid motif are active sites for ion insertion and that this results in ionically repulsive groups facilitating exfoliation. This mechanism is similar to that proposed for the exfoliation of graphene oxide but has rarely been used for COF exfoliation[36] (Fig. S35†). The quinoline-linked covalent organic nanosheets, Qu-CONs, were prepared under mild conditions by immersing the Qu-COFs in a mixture of aqueous 6 M KOH and ethanol (1 : 1) and sonicated for 45 minutes at room temperature. Samples of the representative Im-COFs were prepared in the same way. Suspensions of Qu-CON-1a and Qu-CON-2a exhibited a pronounced Tyndall effect and retained their colloidal stability for up to one week (Fig. 4a, S36 and 37†). The size of the dispersed nanosheets in solution were characterized using dynamic light scattering (DLS). Qu-CON-2a has an average particle size of around 200 nm, which is smaller than that of Qu-CON-1a (around 350 nm) (Fig. S38†). To investigate the morphological properties of the Qu-CON-2a nanosheets, high resolution transmission electron microscopy (HR-TEM) and atomic force microscopy (AFM) were used to probe the layered structure. Qu-CON-2a exhibits a 2D-layered morphology which are thinner than un-exfoliated Qu-COF-2a (Fig. 4b). AFM revealed the 2D sheets have an area of 1–3 μm^2 and thickness of less than 3 nm (Fig. 4c and h). To further probe the effects of the unique quinoline-4-carboxylic acid motif, we performed water contact angles to access wettability. The

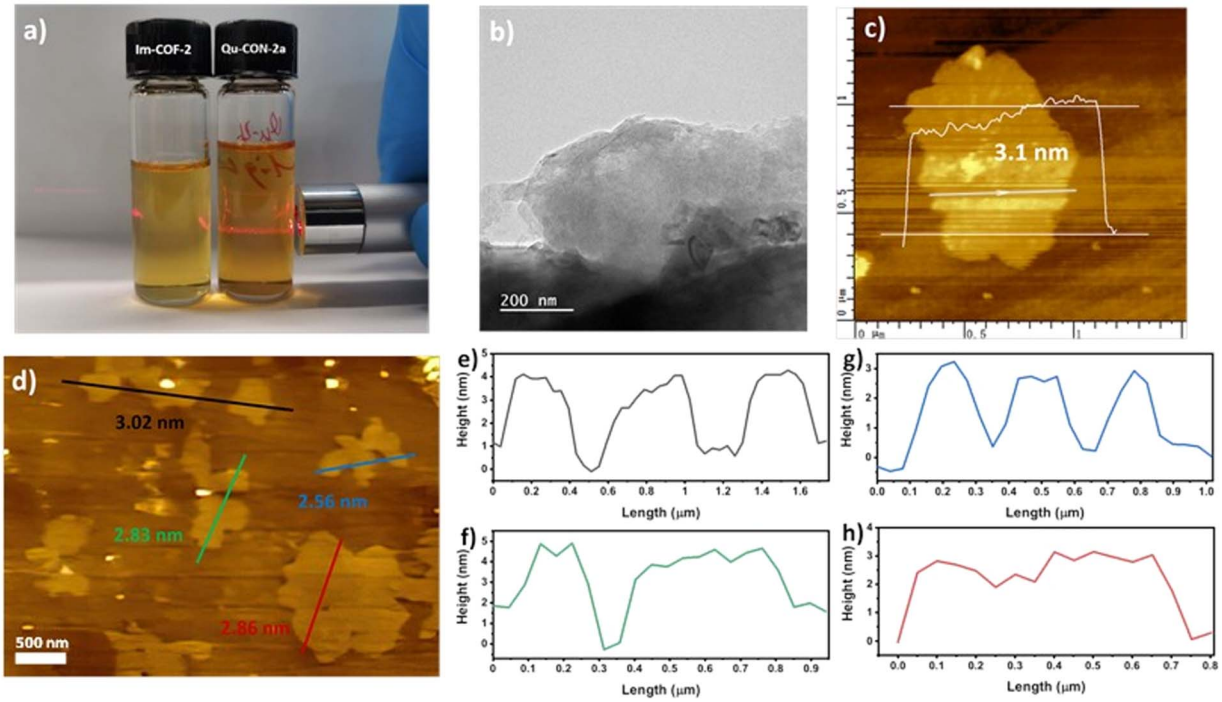

Fig. 4 (a) Images of bulk Im-COF-2 and exfoliated Qu-CON-2a suspension showing Tyndall effect for the latter. (b) HR-TEM image of Qu-CON-2a. (c) AFM image of Qu-CON-2a. Insert is the height of the nanosheet. (d) AFM image of Qu-CON-2a nanosheets with different sizes. Insert is the average height of each nanosheet. (e and h) Corresponding height curves for the selective areas in (d).

hydrophilic carboxylic acid groups greatly enhanced the wettability of Qu-COF-1a and Qu-COF-2a, which is advantageous for exfoliation. By contrast, Im-COF-1a and Im-COF-2a showed water contact angles of ~68° and ~73°, respectively (Fig. S39†).

COFs can be used as adsorbents for the removal of metal ions from polluted solutions, but comparable studies into CONs are rare. Since Qu-CONs have a high concentration of easily accessible quinoline-4-carboxylic groups due to the abundant exposed pores, we decided to investigate metal ion adsorption as a means of water purification. Qu-CON-2a and control samples (Im-COF-2, Qu-COF-2b and Qu-COF-4a) were assayed for the uptake of metal ions from water (Cu^{2+}, Co^{2+}, Ni^{2+}, Zn^{2+}, Cd^{2+}, Eu^{3+}, Pb^{2+}, Mn^{2+} and Mg^{2+}) (Fig. 5a). Compared with Im-COF-2 and Qu-COF-2b, Qu-CON-2a showed a greatly increased uptake for all of these heavy metal ions, especially for Co^{2+}, Ni^{2+}, Zn^{2+} and Cd^{2+}, indicating that the more exposed quinoline-4-carboxylic acid active sites after exfoliation resulted in enhanced adsorption.

Cadmium has the chronic potential to cause kidney, liver, bone and blood damage from long-term exposure at levels above the maximum contaminant level, thus is considered one of the most toxic of the heavy elements found in polluted water.[37] We investigated the adsorption of Cd^{2+} in aqueous solutions between pH 1 to 13 (Fig. 5b). The pH of the solution is important as the protonation and deprotonation property of quinoline-linkages might affect the adsorption behaviour of metals. For Qu-CON-2a, the adsorption of Cd^{2+} increased significantly from 50.78 mg g^{-1} at pH 1 to 99.95 mg g^{-1} at pH 13 when the initial concentration of Cd^{2+} is 100 ppm. At low pH, the quinoline nitrogen atoms are protonated thus resulting in a reduction of Cd^{2+} adsorption. The selectivity of Qu-CON-2a for different metal ions was carried out with the neutral aqueous solutions containing 10 ppm Cu^{2+}, Co^{2+}, Ni^{2+}, Zn^{2+}, Cd^{2+}, Mn^{2+} and Mg^{2+} (Fig. 5c). Qu-CON-2a showed a Cd^{2+} extraction efficiency of around 50%, while the extraction efficiencies of other metal ions were less than 11%, which illustrates that Qu-CON-2a has good selectivity for Cd^{2+}.[38] To further investigate the adsorption behaviour and mechanism of Cd^{2+} adsorption,

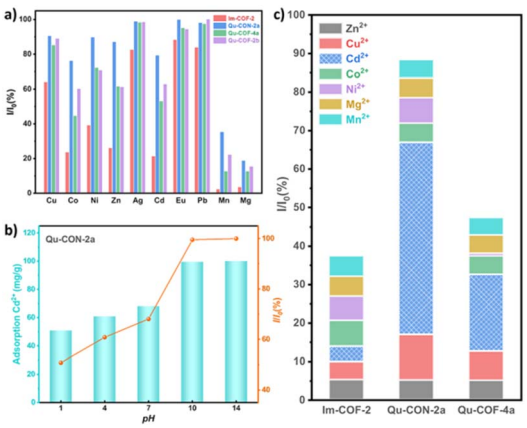

Fig. 5 (a) Adsorption measurements for different metal ions for Im-COF-2 (red), Qu-CON-2a (blue), Qu-COF-4a (green) and Qu-COF-2b (purple). (b) Adsorption of Cd^{2+} by Qu-CON-2a at different pH values (initial concentration of Cd^{2+} is 20 ppm). (c) Adsorption selectivity tests for Im-COF-2, Qu-CON-2a and Qu-COF-4a.

thermodynamic and kinetic experiments were performed using Qu-CON-2a in the neutral aqueous solutions. The adsorption isotherms fit better with the Langmuir model (R^2 of 0.992) than Freundlich model (R^2 of 0.986), indicating the monolayer sorption mechanism (Fig. S40a and b†). The saturated adsorption capacity (Q_m) calculated by the Langmuir equation is 158.7 mg g^{-1}, which is competitive with other reported adsorbents including COFs (Table S3†). The adsorption behaviour of Qu-CON-2a matches well with a pseudo-second-order kinetics model (Fig. S40c and d†), indicating a main driving force of Cd^{2+} adsorption comes from the chemical interaction of the quinoline-4-carboxylic acid.[39] Qu-CON-2a showed a rapid adsorption of Cd^{2+} early on, with the uptakes of 90.0 mg g^{-1} at 1 min and reached up to 97.8% of the adsorption equilibrium within 30 min. To our knowledge, Qu-CON-2a represents the fastest kinetics for the adsorption of Cd^{2+} among COF adsorbents.[40–43] We attribute the fast kinetics to the abundant easily accessible quinoline-4-carboxylic groups after exfoliation. Cadmium-loaded Qu-CON-2a could also be easily separated from solution using a 0.2–0.45 μm syringe filter (area of Qu-CON-2a nanosheets is ~1–3 μm^2), however this is unlikely to be a scalable route for industrial application.

Conclusions

In conclusion, we have developed a simple and efficient multicomponent Doebner synthesis route to stable, porous and crystalline quinoline-linked covalent organic frameworks (Qu-COFs). Post-synthetic modification of imine-based COFs with pyruvic acid was also successful. These Qu-COFs can be exfoliated easily under mild basic conditions owing to the unique quinoline-4-carboxylic acid motif installed using this approach. The quinoline-4-carboxylic acid group has two roles to play in the disruption of interlayer interactions and exfoliation to quinoline-linked covalent organic nanosheets (Qu-CONs): (i) modelling suggests the layers are slightly twisted out of the plane causing larger *d*-spacing, and (ii) ion insertion at the carboxylic group leads to repulsion of the layers. Qu-CONs exhibit excellent performance for cadmium capture from water, with adsorption high capacity, rapid adsorption rates, and good Cd^{2+} selectivity. Our approach provides an efficient way to access robust functional 2D COFs and exfoliated nanosheets, which have promise for applications in selective cadmium adsorption for water purification.

Data availability

No external links have been provided. All supporting data are in the paper and the ESI file provided at submission.†

Author contributions

Y. Xu contributed to the conceptualisation, investigation, materials preparation and characterization, data curation, formal analysis and drafting of the original manuscript. Y. Liu, H. Yang, P. Wang and W. Zhang contributed to the investigation. X. Wang contributed to the software. J. W. Ward handled project administration, supervision and revised the manuscript. A. I. Cooper supervised the work and revised the manuscript. All authors have approved the final version of the manuscript.

Conflicts of interest

There are no conflicts to declare.

Acknowledgements

This work was financially supported by the Leverhulme Trust *via* the Leverhulme Research Centre for Functional Materials Design. The authors thank Dr Marco Zanella, Dr Haiyan Duan, and Dr Kai Wu for valuable input on the AFM experiments and Dr Kewei Wang for the useful discussions. Weiwei Zhang acknowledges support from the Science and Technology Commission of Shanghai Municipality (24160711900).

References

1 C. S. Diercks and O. M. Yaghi, *Science*, 2017, **355**, eaal1585.
2 H. Furukawa and O. M. Yaghi, *J. Am. Chem. Soc.*, 2009, **131**, 8875–8883.
3 H. Oh, S. B. Kalidindi, Y. Um, S. Bureekaew, R. Schmid, R. A. Fischer and M. Hirscher, *Angew. Chem., Int. Ed.*, 2013, **52**, 13219–13222.
4 S. Lu, Y. Hu, S. Wan, R. McCaffrey, Y. Jin, H. Gu and W. Zhang, *J. Am. Chem. Soc.*, 2017, **139**, 17082–17088.
5 M. Bhadra, S. Kandambeth, M. K. Sahoo, M. Addicoat, E. Balaraman and R. Banerjee, *J. Am. Chem. Soc.*, 2019, **141**(15), 6152–6156.
6 X. Wang, L. Chen, S. Y. Chong, M. A. Little, Y. Wu, W.-H. Zhu, R. Clowes, Y. Yan, M. A. Zwijnenburg, R. S. Sprick and A. I. Cooper, *Nat. Chem.*, 2018, **10**, 1180–1189.
7 C. R. DeBlase, K. E. Silberstein, T.-T. Truong, H. C. D. Abruña and W. R. Dichtel, *J. Am. Chem. Soc.*, 2013, **135**, 16821–16824.
8 E. Vitaku, C. N. Gannett, K. L. Carpenter, L. Shen, H. D. Abruña and W. R. Dichtel, *J. Am. Chem. Soc.*, 2020, **142**(1), 16–20.
9 F. Haase, K. Gottschling, L. Stegbauer, L. S. Germann, R. Gutzler, V. Duppel, V. S. Vyas, K. Kern, R. E. Dinnebier and B. V. Lotsch, *Mater. Chem. Front.*, 2017, **1**, 1354–1361.
10 H. Lyu, C. S. Diercks, C. Zhu and O. M. Yaghi, *J. Am. Chem. Soc.*, 2019, **141**, 6848–6852.
11 E. Jin, M. Asada, Q. Xu, S. Dalapati, M. A. Addicoat, M. A. Brady, H. Xu, T. Nakamura, T. Heine, Q. Chen and D. Jiang, *Science*, 2017, **357**, 673–676.
12 K. Wang, L. M. Yang, X. Wang, L. Guo, G. Cheng, C. Zhang, S. Jin, B. Tan and A. I. Cooper, *Angew. Chem., Int. Ed.*, 2017, **56**, 14149–14153.
13 J. Guo, Y. Xu, S. Jin, L. Chen, T. Kaji, Y. Honsho, M. A. Addicoat, J. Kim, A. Saeki, H. Ihee, S. Seki, S. Irle, M. Hiramoto, J. Gao and D. Jiang, *Nat. Commun.*, 2013, **4**, 1–8.
14 P.-F. Wei, M.-Z. Qi, Z.-P. Wang, S.-Y. Ding, W. Yu, Q. Liu, L.-K. Wang, H.-Z. Wang, W.-K. An and W. Wang, *J. Am. Chem. Soc.*, 2018, **140**, 4623–4631.

15 D. W. Burke, C. Sun, X. Wang, I. Castano, N. C. Flanders, A. M. Evans, E. Vitaku, D. C. McLeod, R. H. Lambeth, L. Chen, N. C. Gianneschi and W. R. Dichtel, *Angew. Chem., Int. Ed.*, 2019, **132**, 5203–5209.
16 K. Li, N. K. Wong, M. J. Strauss, A. M. Evans, M. Matsumoto, W. R. Dichtel and A. Adronov, *J. Am. Chem. Soc.*, 2021, **143**, 649–656.
17 D. A. Pyles, W. H. Coldren, G. M. Eder, C. M. Hadad and P. L. McGrier, *Chem. Sci.*, 2018, **9**, 6417–6423.
18 B. Zhang, M. Wei, H. Mao and X. Pei, *J. Am. Chem. Soc.*, 2018, **140**, 12715–12719.
19 X. Guan, H. Li, Y. Ma, M. Xue, Q. Fang and Y. Yan, *Nat. Chem.*, 2019, **11**, 587–594.
20 S. Dalapati, S. Jin, J. Gao, Y. Xu, A. Nagai and D. Jiang, *J. Am. Chem. Soc.*, 2013, **135**, 17310–17313.
21 S. Kandambeth, A. Mallick, B. Lukose, M. V. Mane, T. Heine and R. Banerjee, *J. Am. Chem. Soc.*, 2012, **134**, 19524–19527.
22 H. Liu, J. Chu, Z. Yin, X. Cai, L. Zhuang and H. Deng, *Chem*, 2018, **4**, 1696–1709.
23 P. J. Waller, S. J. Lyle, T. M. Osborn Popp, C. S. Diercks, J. A. Reimer and O. M. Yaghi, *J. Am. Chem. Soc.*, 2016, **138**, 15519–15522.
24 P. J. Waller, Y. S. AlFaraj, C. S. Diercks, N. N. Jarenwattananon and O. M. Yaghi, *J. Am. Chem. Soc.*, 2018, **140**, 9099–9103.
25 X. Li, C. Zhang, S. Cai, X. Lei, V. Altoe, F. Hong, J. J. Urban, J. Ciston, E. M. Chan and Y. Liu, *Nat. Commun.*, 2018, **9**, 1–8.
26 B. B. Toure and D. G. Hall, *Chem. Rev.*, 2009, **109**, 4439–4486.
27 P.-L. Wang, S.-Y. Ding, Z.-C. Zhang, Z.-P. Wang and W. Wang, *J. Am. Chem. Soc.*, 2019, **141**, 18004–18008.
28 K. Wang, Z. Jia, Y. Bai, X. Wang, S. E. Hodgkiss, L. Chen, S. Chong, H. Yang, Y. Xu, F. Feng, J. W. Ward and A. I. Cooper, *J. Am. Chem. Soc.*, 2020, **142**, 11131–11138.
29 X.-T. Li, J. Zou, T. H. Wang, H.-C. Ma, G.-J. Chen and Y.-B. Dong, *J. Am. Chem. Soc.*, 2020, **142**(14), 6521–6526.
30 F. Haase, E. Troschke, G. Savasci, T. Banerjee, V. Duppel, S. Dörfler, M. M. J. Grundei, A. M. Burow, C. Ochsenfeld, S. Kaskel and B. V. Lotsch, *Nat. Commun.*, 2018, **9**, 1–10.
31 C. Li, Y. Ma, H. Liu, L. Tao, Y. Ren, X. Chen, H. Li and Q. Yang, *Chinese J. Catal.*, 2020, **41**, 1288–1297.
32 S. Yamashkin and E. Oreshkina, *Chem. Heterocycl. Compd.*, 2006, **42**, 86–91.
33 X. Sui, Y. Wang, F. Liu, Z. Yuan, C. Wang, Y. Yu, K. Zhou, K. Goh and Y. Chen, *Matter*, 2021, **4**, 2953–2969.
34 Y. Yang, L. Yu, T. Chu, H. Niu, J. Wang and Y. Cai, *Nat. Commun.*, 2022, **13**, 2615.
35 P. Das, G. Chakraborty, J. Roeser, S. Vogl, J. Rabeah and A. Thomas, *J. Am. Chem. Soc.*, 2023, **145**, 2975–2984.
36 Y. Tao, W. Ji, X. Ding and B. Han, *J. Mater. Chem. A*, 2021, **9**, 7336–7365.
37 X. Liu, H. Pang, X. Liu, Q. Li, N. Zhang, L. Mao, M. Qiu and B. Hu, *Innovation*, 2021, **2**, 100076.
38 L. Guo, S. Jia, C. Diercks, X. Yang, S. Alshmimri and O. M. Yaghi, *Angew. Chem., Int. Ed.*, 2020, **132**, 2039–2043.
39 Z. Li, R. Zhu, P. Zhang, M. Yang, R. Zhao, Y. Wang, X. Dai and W. Liu, *Chem. Eng. J.*, 2022, **434**, 134623.
40 V. D. da Silva, K. Zalewska, Z. Petrovski, C. D. Buarque, L. C. Branco and P. M. Esteves, *Mater. Today. Sustain.*, 2023, **21**, 100279.
41 E. Gendy, J. Ifthikar, J. Ali, D. T. Oyekunle, Z. Elkhlifa, I. I. Shahib, A. I. Khodair and Z. Chen, *J. Environ. Chem. Eng.*, 2021, **9**, 105687.
42 N. Liu, L. Shi, X. Han, Q.-Y. Qi, Z.-Q. Wu and X. Zhao, *Chin. Chem. Lett.*, 2020, **31**, 386–390.
43 W. L. Jin, W. Li, H. X. Wang, X. W. Liu, H. X. Jiang, L.-N. Zhu and D. M. Kong, *J. Environ. Chem. Eng.*, 2022, **10**, 107662.

